JOURNAL OF GEOPHYSICAL RESEARCH, VOL. 97, NO. C10, PAGES 15,467–15,480, OCTOBER 15, 1992

Large-Scale Electric and Magnetic Fields Generated by the Oceans

DAVID STEPHENSON[1]

Atmospheric and Oceanic Sciences Program, Princeton University, Princeton, New Jersey

KIRK BRYAN

Geophysical Fluid Dynamics Laboratory, NOAA, Princeton, New Jersey

The magnetostatic equations are used to derive a consistent set of equations capable of describing the global-scale, low-frequency electric and magnetic fields induced by the motion of the ocean through the geomagnetic field. The equations are solved numerically with realistic 2° × 2° topography in a global domain with ocean flow simulated by a detailed ocean circulation model. Estimates of the annual mean and the first annual harmonic of the electric potential, the vertical component of the oceanic magnetic field, and the vertically integrated electric current density stream function are obtained. With the idea of using electric and magnetic fields to deduce large-scale oceanic flow, emphasis is placed on the geographical location of interesting features. The fields are not found to be basin-wide but rather are found to be localized and strongest in shallow regions. The magnetic fields generated by ocean currents are of the order of 1 nT, and while these can be measured by magnetometers, they would be difficult to detect owing to contamination from other sources of magnetic variation. In finding the electric field, electric currents cannot be neglected where ocean currents cut across isobaths. However, in regions where the ocean flow is aligned with the isobaths, measurement of electric fields is sufficient to find the ocean flow.

1. INTRODUCTION

Ever since *Faraday* [1832] attempted to measure the flow of the River Thames by measuring the potential across electrodes lowered from Waterloo Bridge, people have been attempting to use motionally induced electric and magnetic fields to deduce geophysical flows. Salt in the ocean makes it a good conductor. The movement of a conductor through a magnetic field induces a potential drop across the conductor proportional to the product of its velocity and the magnetic field. Depending on the geometry, this can in turn cause electric currents to flow in the conductor. The electric currents give rise to a secondary magnetic field. The inverse problem is to deduce the flow field given either the electric field or the magnetic field or both. Depending on the situation, both fields may be necessary. The direct problem is to calculate the electric and magnetic fields given the flow.

Over the last century, magnetic observatories around the globe have been continuously monitoring the Earth's magnetic field, and if these data could somehow be inverted, they would be a valuable source of information on the ocean flow. Also, it has been reported (S. K. Runcorn, personal communication, 1991) that analyzed observatory data show a magnetic signal coming from the interior which has an annual cycle and is spatially correlated with the ocean basins. Unfortunately, little is known about how to invert these data to obtain ocean flows globally. This is a motivation to do theoretical studies aimed at understanding how the ocean currents are related to motionally generated electric and magnetic fields on large spatial scales and seasonal time scales.

Furthermore, measurements of electric fields using undersea communication cables, towed electrodes, and seabed devices have been performed. Comparison of total transports of the Florida Current deduced from cable measurements and from current meter mooring and profiling observations indicate that cable measurements can be a very good way to measure ocean transports over a wide range of time scales [*Larsen*, 1992]. A detailed comparison of measurements of a bottom-mounted device and current meter data has recently been carried out [*Chave and Luther*, 1990; *Luther et al.*, 1991].

Theoretical work on the electromagnetic behavior of the oceans has been performed over the last 40 years (refer to *Larsen* [1992] for a complete review). The direct problem is in principle simple, but the effects of varying topography and conductivity variations within both the sea and the seabed complicate the problem. No attempt has been made to calculate the electromagnetic behavior for the global domain with realistic ocean flows and topography. It is our belief that this is a necessary first step. Such a large-scale view has the problem that it is incapable of addressing small-scale phenomena in the electric and magnetic fields. However, it provides a description of the global behavior and can be used to find interesting regions for smaller-scale studies. For example, regions of strong electric fields can be identified which can then be of use in choosing cables which provide good measurements. Another advantage of a global study is that it requires no boundary conditions in the horizontal directions. This is of special importance in calculating the global magnetic field due to the ocean. Smaller-domain studies have to make some assumptions about the electric currents on the horizontal boundaries.

In this paper we aim to understand the global electric and magnetic fields motionally induced by oceanic flow on seasonal time scales. Our model is incapable of describing scales less than about 4° and is intended to represent the

[1]Now at Department of Meteorology, University of Reading, Reading, England.

Paper number 92JC01400.
0148-0227/92/92JC-01400$05.00

global picture rather than the fine detail. In sections 2–4 we start from the magnetostatic equations and derive a simple, vertically averaged thin-shell equation appropriate for large scales and low frequency. We model the ocean and adjacent land areas as a thin conductive shell between two perfect insulating layers, one representing the atmosphere above and the other representing the upper mantle below. Furthermore, we simplify the conductivity distribution to one having only two values, one for land and one for sea. This is all done in order to obtain an equation which can be easily solved numerically and which contains the essential behavior of the motionally induced fields. Our model is roughly consistent with what little is known, but for simplicity it neglects effects which may be important quantitatively. For example, the fact that saturated ocean sediments have a much higher conductivity than solid crust is ignored, as are conducting layers at deeper levels in the mantle [*Mackie et al.*, 1988; *Cox et al.*, 1986]. In section 6 we describe how we solved the equation numerically. Section 7 explains the ocean model used for the flow field. We present the results of the simulation in section 8 and conclude with a discussion in section 9.

2. Magnetostatic Equations: Derivation From Maxwell's Equations

Under the assumption that the time period of interest T is such that $T \gg \varepsilon/\sigma$, where ε is the relative permittivity and σ is the electrical conductivity of the medium, the displacement currents are much less than the total electric currents, and electromagnetic radiation is negligible. Under these conditions, Maxwell's equations for a moving medium become [*Sanford*, 1971]

$$\partial \mathbf{B}/\partial t = -\nabla \Lambda \mathbf{E} \tag{1}$$

$$\mathbf{E} = K\mu \mathbf{J} - \mathbf{v} \Lambda \mathbf{B} \tag{2}$$

$$\mu \mathbf{J} = \nabla \Lambda \mathbf{B} \tag{3}$$

These are known as the magnetostatic equations for a medium with magnetic permeability μ. The magnetic diffusivity $K = (\sigma\mu)^{-1}$ acts as a diffusion coefficient for the magnetic field.

Equations (1)–(3) can be combined to give

$$\partial \mathbf{B}/\partial t = -\nabla \Lambda (K \nabla \Lambda \mathbf{B} - \mathbf{v} \Lambda B) \tag{4}$$

Furthermore, we can split $\mathbf{B}$ into the field $\mathbf{b}$ due to the oceans and the geomagnetic field $\mathbf{F}$, i.e., $\mathbf{B} = \mathbf{F} + \mathbf{b}$. Omitting time variations in $\mathbf{F}$ and using the fact that $\nabla \Lambda \mathbf{F} = 0$ (i.e., away from geomagnetic current sources), we obtain the equation

$$\partial \mathbf{b}/\partial t = -\nabla \Lambda (K \nabla \Lambda \mathbf{b}) + \nabla \Lambda (\mathbf{v} \Lambda \mathbf{b}) + \nabla \Lambda (\mathbf{v} \Lambda \mathbf{F}) \tag{5}$$

This has four terms, which are the "self-induction" term $\partial \mathbf{b}/\partial t$, the "resistive term" $-\nabla \Lambda (K \nabla \Lambda \mathbf{b})$, the "dynamo term" $\nabla \Lambda (\mathbf{v} \Lambda \mathbf{b})$, and the "motional induction term" $\nabla \Lambda (\mathbf{v} \Lambda \mathbf{F})$.

3. Thin-Shell Approximation

The physical model which will be the basis of our calculations is that of a spherical shell whose outer radius is the surface of the oceans and whose inner radius corresponds to the maximum depth of the oceans. In our model we assume that the atmosphere above the shell and the crust below the shell are perfect insulators.

With the exception of lightning strikes, the atmosphere is much less conducting than the saltwater in the ocean, and hence it is a good approximation to treat it as a perfect insulator. The case of the earth beneath the ocean is much harder to justify. Although the conductivity of the crust and mantle is much less than that of seawater, the crust-mantle system can provide a return path for electric currents generated in the ocean by virtue of the larger cross-sectional area available to electric currents flowing into the earth beneath the sea than to those flowing through the sea. This simplistic argument is complicated by the fact that current paths are refracted at the interface of media having different conductivities. In this paper we neglect the complication involved in having more than two layers of differing conductivity and make the assumption that leakage currents throughout the lithosphere are negligible to those through the sea. (Work is in progress by A. Flosadottir at Seattle on the multilayer problem.)

Let the outer radius of the shell be a, the radius of the Earth, and the inner radius be $a - D$. The radius of the Earth is an appropriate horizontal scale for ocean circulation so that the aspect ratio of the model, δ, is

$$\delta = D/a \tag{6}$$

where δ is approximately 10^{2-3}.

Another factor of importance is the ratio of the induced field in the oceans and the Earth's geomagnetic field. We define this as β, where

$$\beta = b_0/F_0 \tag{7}$$

Theoretical estimates of b_0, the typical magnitude of $\mathbf{b}$, are less than 20 nT [*Chapman and Bartels*, 1940], whereas F_0 is a typical value for the geomagnetic field of 4×10^4 nT. Thus β is of the order of 5×10^{-4}.

The ratio of advection of the magnetic field to diffusion is called the magnetic Reynolds number, R_m where

$$R_m = U_0 a/K \tag{8}$$

For the ocean the conductivity is of the order of $4\ \Omega^{-1}\ \mathrm{m}^{-1}$ and μ is equal to $4\pi \times 10^{-7}$, giving a K of the order of $2 \times 10^5\ \mathrm{m}^2\ \mathrm{s}^{-1}$. The radius of the Earth is 6.37×10^6 m, and a typical ocean velocity is $0.1\ \mathrm{m\ s}^{-1}$. Thus R_m is typically of the order of unity.

This result implies that advection is as equally important as diffusion. However, diffusion occurs isotropically, and hence diffusion in the vertical should also be considered. This has the effect of replacing the horizontal length scale a in R_m by the vertical length scale D. It can then be seen that the vertical magnetic Reynolds number is a factor of a thousand less than the horizontal one, which implies that vertical diffusion dominates both horizontal diffusion and advection. This is shown formally in Appendix A. Over land the velocity is zero, and hence the diffusion term is the only term; the equations approximate to Laplace's equation over land.

In Appendix A, equation (5) is written in nondimensional form and an expansion is made with respect to the small parameters β and δ. At zero order, the magnetostatic equations in dimensional form are

$$\partial_z e_\phi = 0 \tag{9}$$

$$\partial_z e_\lambda = 0 \tag{10}$$

$$\frac{1}{\cos\phi}\partial_\lambda e_\phi - \frac{1}{\cos\phi}\partial_\phi(e_\lambda \cos\phi) = 0 \tag{11}$$

$$e_\phi = +K\partial_z b_\lambda + uF_z \tag{12}$$

$$e_\lambda = -K\partial_z b_\phi - vF_z \tag{13}$$

where b_λ and b_ϕ are zonal and meridional components of the induced magnetic fields and F_z is the vertical component of the geomagnetic field. Equations (9)–(13) are the appropriate thin-shell approximation of the magnetostatic model for monthly to annual time scales. Since all omitted terms are of the order of β or δ, and these parameters are of the order 10^{-3}, we see that the thin-shell approximation is very accurate and little would be gained from using the full magnetostatic equations shown in (4). Note that the equations contain no time derivatives and so the only time dependence comes from time variations in the ocean flow field (u, v).

4. Vertical Integration

We wish to use equations (9)–(13) to calculate the magnetic fields measurable at magnetic stations situated outside of the thin shell, i.e., $r > a$. In the insulating interior ($r < a - D$) and exterior ($r > a$) regions, the magnetic field is given by the gradient of a potential field Ω which satisfies $\nabla^2\Omega = 0$. The effect of electric currents in the thin shell is to cause a magnetic potential drop χ across the thin shell situated at $r = a$. Calculating χ from our knowledge of the ocean flow and using suitable boundary conditions, we can find Ω and hence the magnetic field everywhere. As the thin shell approaches zero thickness, suitable boundary conditions for Ω become $\Omega|^a_{r=a-D} = \chi$, $\partial_r\Omega|^a_{r=a-D} = 0$ and Ω must be finite as $r \to 0$ and $r \to \infty$. Given χ, these conditions can be most easily solved by expanding Ω in terms of spherical harmonics and then solving for the coefficients (refer to Appendix B for details).

To be able to find an expression for χ, we must vertically integrate (12) and (13) from $z = -D$ to $z = 0$, and we find that

$$e_\phi = \frac{K_{\text{eff}}}{D}\left(b_\lambda|^0_{-D} + \int_{-D}^{0}\frac{uF_z}{K}\,dz\right) \tag{14}$$

$$e_\lambda = -\frac{K_{\text{eff}}}{D}\left(b_\phi|^0_{-D} + \int_{-D}^{0}\frac{vF_z}{K}\,dz\right) \tag{15}$$

$$K_{\text{eff}}^{-1} = \frac{1}{D}\int_{-D}^{0}\frac{dz}{K} \tag{16}$$

Note that $K_{\text{eff}}^{-1} = \langle\sigma\rangle\mu$, where $\langle\sigma\rangle$ is a depth-averaged conductivity as discussed by *Sanford* [1971]. In deriving these expressions, we have made use of (9) and (10) which state that for thin shells the horizontal components of the electric field do not vary with depth.

To proceed further, we make an assumption about the depth variation of K. We assume that K can take only two values:

$$\begin{aligned} K &= K_S \qquad 0 \geq z > -d \\ K &= K_L \qquad -d \geq z \geq -D \end{aligned} \tag{17}$$

Depth d is the depth of the ocean and is always less than or equal to D.

We note that

$$K_{\text{eff}}^{-1} = \mu[d\sigma_S + (D - d)\sigma_L]/D$$

where the left-hand side is μ times the depth-averaged conductivity as defined by the model.

The sea and land values K_S and K_L have typical values of 2×10^5 m^2 s^{-1} and 2×10^8 m^2 s^{-1} [*Larsen*, 1992]. The conductivity of seawater depends on both temperature and salinity and this may play a role in the variability of the oceanic magnetic and electric fields. (Recent work by J. Girton indicates that inclusion of conductivity variability does not change the results from those presented in this paper.) However, in this paper we consider the variations in K_S to be small in comparison to the factor of 1000 between K_L and K_S, and hence we neglect variations in K_S.

With the reasonable rigid-lid approximation, the vertically averaged ocean flow can be written in terms of a stream function. Furthermore, we will neglect depth variations in F_z which are small because of the spherical shell's being thin. These assumptions allow us to write

$$\int_{-D}^{0}\frac{uF_z}{K}\,dz = \frac{-F_z}{K_S a}\frac{\partial\psi}{\partial\phi} \tag{18}$$

$$\int_{-D}^{0}\frac{vF_z}{K}\,dz = \frac{F_z}{K_S a\cos\phi}\frac{\partial\psi}{\partial\lambda} \tag{19}$$

where ψ is a time-varying transport stream function for the ocean which varies with time. Substituting these expressions into (14) and (15) gives

$$e_\phi = \frac{K_{\text{eff}}}{D}\left(\frac{1}{a\cos\phi}\frac{\partial\chi}{\partial\lambda} - \frac{F_z}{K_S a}\frac{\partial\psi}{\partial\phi}\right) \tag{20}$$

$$e_\lambda = -\frac{K_{\text{eff}}}{D}\left(\frac{1}{a}\frac{\partial\chi}{\partial\phi} + \frac{F_z}{K_S a\cos\phi}\frac{\partial\psi}{\partial\lambda}\right) \tag{21}$$

$$K_{\text{eff}} = D\left(\frac{d}{K_S} + \frac{D - d}{K_L}\right)^{-1} \tag{22}$$

Equations (20) and (21) can be substituted into (11) to yield

$$\nabla\cdot(K_{\text{eff}}\nabla\chi) + J\left(\psi, \frac{K_{\text{eff}}}{K_S}F_z\right) = 0 \tag{23}$$

with the two-dimensional operators defined as

$$\nabla\chi = \left(\frac{1}{a\cos\phi}\frac{\partial\chi}{\partial\lambda}, \frac{1}{a}\frac{\partial\chi}{\partial\phi}\right) \tag{24}$$

$$\nabla\cdot(f_\lambda, f_\phi) = \frac{1}{a\cos\phi}\frac{\partial f_\lambda}{\partial\lambda} + \frac{1}{a\cos\phi}\frac{\partial}{\partial\phi}(f_\phi\cos\phi) \tag{25}$$

$$J(f, g) = \frac{1}{a \cos \phi} \frac{\partial f}{\partial \lambda} \frac{1}{a} \frac{\partial g}{\partial \phi} - \frac{1}{a \cos \phi} \frac{\partial g}{\partial \lambda} \frac{1}{a} \frac{\partial f}{\partial \phi} \quad (26)$$

Equation (23) relates the magnetic potential drop χ, which is a stream function for the vertically averaged electric currents, to the stream function ψ for the vertically averaged ocean flow. In the next section we will solve (23) numerically for given ψ in order to find χ. The vertical component of the magnetic field strength at sea level, b_z, can be obtained from χ as described in Appendix B.

Another quantity of interest is the electric potential Φ defined by $\nabla\Phi = (e_\lambda, e_\phi)$. The potential Φ can be obtained by taking the divergence of $\nabla\Phi$ to yield $\nabla^2\Phi = -\nabla \cdot (e_\lambda, e_\phi)$ and then inverting the two dimensional Laplacian (using spherical harmonics). The expressions for (e_λ, e_ϕ) are obtained from (20) and (21). The potential Φ is of relevance to the measurement of voltages across underwater telephone cables. If a cable runs from point A to point B, then the voltage drop across the cable is equal to $\Phi_B - \Phi_A$. Hence the global distribution of Φ is of importance in choosing optimum cables for measuring ocean flow.

5. General Properties

Scale Analysis

Scale analysis of the equations in section 4 gives

$$\chi \approx (F_z/K)\psi \quad (27)$$

$$b_z \approx (F_z\psi/KL) \quad (28)$$

$$\Phi \approx (F_z\psi/D) \quad (29)$$

where ψ is the volume transport of an ocean current with a depth D and a width L. Consider the Florida Current, where the time mean $\psi \approx 30 \times 10^6$ m^3 s^{-1}, D is $\approx$800 m, and L is $\approx$300 km. In this region, $F_z \approx 40{,}000$ nT and $K \approx 2 \times 10^5$ m^2 s^{-1}. Using these values gives $\chi \approx 6 \times 10^6$ nT, $b_z \approx 20$ nT, and $\Phi \approx 1.5$ V. The value for the ocean magnetic field of 20 nT agrees with that calculated by *Chapman and Bartels* [1940, p. 709]. Equation (29) can be written in terms of a sverdrup-to-volt conversion factor $C = 10^{-6}D/F_z$ [*Larsen*, 1992]. With the values given above we get $C = 20$ Sv V^{-1} compared with the measured value of 24.4 Sv V^{-1} discussed by Larsen.

Uniform Geomagnetic Field and Topography

In the case that $(K_{\text{eff}}/K_S)F_z$ is constant with (λ, ϕ), the Jacobian term vanishes, leaving only the diffusion term. The solution on a sphere is a uniform χ field. Hence spatial variation of the geomagnetic field and bottom topography is a necessary requirement for the ocean to generate a magnetic field. This is used as a check in the numerical code mentioned in section 6.

6. Method of Solution

The thin-shell approximation and vertical integration reduce the problem to the second-order elliptic partial differential equation in two dimensions given by (23) in section 5. Let $i = 1, 2, \cdots$ represent the index of grid points in the zonal direction and j denote the index of grid points in the meridional direction. To simplify the notation, we define the following numerical operators:

$$\delta_\lambda = [(\ )_{i+1/2} - (\ )_{i-1/2}]/\Delta\lambda \quad (30)$$

$$(\ )^\lambda = [(\ )_{i+1/2} + (\ )_{i-1/2}]/2 \quad (31)$$

Instead of defining every variable at every grid point, we use a staggered grid. In this way, variables are defined where they are required by second-order finite differencing of the continuous equations. The redundancy which occurs when every variable is defined at every grid point is avoided. If we think of the numerical grid as a checkboard, χ and ψ are defined at the center of the squares, and e_λ and e_ϕ are defined at the corner points. Special care must be taken in defining derivatives because the grid of the ocean model from which the values of ψ are taken has uneven spacing in the meridional direction. Equations (20) and (21) can be written,

$$e_\lambda = -\frac{K_{\text{eff}}}{D}\left(\frac{1}{a}\delta_\phi\langle\chi\rangle^\lambda + \frac{\langle F_z\rangle^{\phi\lambda}}{K_S a \cos\phi}\frac{\delta_\lambda\langle\psi\Delta\phi\rangle^\phi}{\langle\Delta\phi\rangle^\phi}\right) \quad (32)$$

$$e_\phi = \frac{K_{\text{eff}}}{D}\left(\frac{1}{a\cos\phi}\frac{\delta_\lambda\langle\chi\Delta\phi\rangle^\phi}{\langle\Delta\phi\rangle^\phi} - \frac{\langle F_z\rangle^{\phi\lambda}}{K_S a}\delta_\phi\langle\psi\rangle^\lambda\right) \quad (33)$$

Equation (23) may then be represented as

$$L\chi = G \quad (34)$$

where L is a numerical representation of a diffusion operator with nonconstant coefficients.

$$L\chi = \frac{\delta_\lambda\{\{K_{\text{eff}}/D[(1/a\cos\phi)(\delta_\lambda\langle\chi\Delta\phi\rangle^\phi/\langle\Delta\phi\rangle^\phi)]\}\Delta\phi\rangle^\phi}{\langle\Delta\phi\rangle^\phi} + \delta_\phi\left\{\left\langle\left[\frac{K_{\text{eff}}}{D}\left(\frac{1}{a}\delta_\phi\langle\chi\rangle^\lambda\right)\right]\right\rangle^\lambda\cos\phi\right\} \quad (35)$$

G is simply the forcing term involving the second terms on the right-hand sides of (32) and (33). A simple iterative method, corresponding to under relaxation, was used to solve (35).

$$\chi^{n+1} = \chi^n + \alpha(L\chi^n - G) \quad (36)$$

This iterative method is exactly analogous to a simple time-marching, thermal diffusion problem. The stability criterion [*Richtmyer and Morton*, 1967] is well known.

$$\alpha \frac{K_{\text{eff}}}{Da^2\cos\phi(\Delta\lambda)^2} \leq \frac{1}{2} \quad (37)$$

This criterion is most restrictive as the meridians converge to the poles. To avoid the extremely small α required near the poles, Fourier filtering is performed in the zonal direction so as to cut off all zonal scales less than that of the zonal grid spacing at the equator.

To calculate G, the fields ψ and F_z are required. In addition, the parameters K_L and K_S and the depth of the ocean are required in order to calculate K_{eff}/K_S. For the geomagnetic field F_z, we use the 1980 values given in Table 1 and shown in Figure 1 taken from *Merrill and McElhinney* [1983]. For the ocean stream function we take 12 monthly values from the ocean model described in the next section.

TABLE 1. Gauss Coefficients

l	m	G	H	g	h	g'	h'
1	0	−30001.01	0.00	50.93	0.00	4.23	0.00
1	1	−1949.99	5634.00	160.47	286.40	5.00	6.33
2	0	−2038.01	0.00	80.61	0.00	5.77	0.00
2	1	3035.01	−2134.00	−211.02	−272.61	2.25	8.90
2	2	1652.00	−179.00	−13.29	3.58	2.41	6.21
3	0	1292.99	0.00	−86.37	0.00	5.08	0.00
3	1	−2155.98	−38.00	171.60	145.49	1.25	2.71
3	2	1244.00	261.00	99.58	−0.17	7.08	3.01
3	3	851.00	−235.00	−10.50	12.38	2.40	4.35
4	0	918.99	0.00	43.07	0.00	1.56	0.00
4	1	777.02	189.00	−52.84	−30.52	4.12	2.45
4	2	411.00	−265.00	−89.09	−51.92	3.74	1.63
4	3	−428.00	69.00	43.98	4.21	1.55	4.49
4	4	224.00	−289.00	22.33	−72.09	1.93	7.93
5	0	−216.01	0.00	−60.76	0.00	2.93	0.00
5	1	354.03	74.00	−50.04	−32.85	1.50	2.98
5	2	261.00	147.00	23.80	13.33	4.03	4.73
5	3	−66.00	−149.00	−37.13	−12.67	3.02	5.10
5	4	−173.00	−71.00	7.97	43.93	1.43	2.76
5	5	−52.00	101.00	42.28	−4.74	5.78	2.33
6	0	50.99	0.00	46.32	0.00	1.48	0.00
6	1	57.03	−15.00	107.52	99.12	6.42	3.22
6	2	47.00	98.00	4.24	−23.06	2.49	2.19
6	3	−194.00	75.00	−5.99	11.10	4.41	2.90
6	4	6.00	−44.00	−61.48	−59.46	2.59	5.16
6	5	17.00	2.00	−76.96	7.97	3.10	3.20
6	6	−104.00	27.00	−5.10	−1.89	3.88	2.66
7	0	64.99	0.00	−1.99	0.00	1.75	0.00
7	1	−54.96	−70.99	−108.86	−96.71	2.47	0.83
7	2	7.00	−24.00	−38.00	41.64	5.46	5.39
7	3	17.00	9.00	−10.92	25.12	1.98	1.10
7	4	−17.00	8.00	56.05	31.69	5.28	1.47
7	5	−1.00	12.00	64.31	−6.68	2.12	2.90
7	6	16.00	−17.00	13.01	5.88	2.38	3.96
7	7	9.00	−14.00	−3.83	−0.68	1.75	4.01
8	0	12.99	0.00	10.76	0.00	3.18	0.00
8	1	8.04	12.01	48.60	77.11	4.04	1.11
8	2	−4.00	−21.00	52.07	−12.52	0.91	2.81
8	3	−5.00	11.00	26.72	−35.05	2.72	0.09
8	4	−12.00	−20.00	−56.51	11.32	1.98	2.46
8	5	0.00	10.00	−58.09	41.46	3.98	0.46
8	6	−1.00	7.00	−43.98	−12.66	0.97	2.01
8	7	10.00	−13.00	12.95	−2.26	1.99	3.07
8	8	3.00	−13.00	−10.88	1.60	4.28	2.54

G and H are in nanoteslas. All others are in picoteslas. G and H are those for the 1980 Geomagnetic Field, g and h are the annual mean ocean magnetic field, and g' and h' are the magnitudes of the annual fluctuations.

The depth of the ocean also comes from the ocean model. For K_S we use the value 2×10^5 m^2 s^{-1} corresponding to an ocean conductivity of 4 Ω^{-1} m^{-1}. For K_L we used the values 2×10^5, 2×10^6, 4×10^6, 6×10^6, 8×10^6, and 10^7 m^2 s^{-1} corresponding to land conductivities of 4, 0.4, 0.2, 0.13, 0.1, and 0.08 Ω^{-1} m^{-1}, respectively. Ideally, to model land realistically, we would like to use a value of $K_L = 2 \times 10^8$ m^2 s^{-1} corresponding to a conductivity of 0.004 Ω^{-1} m^{-1}. Unfortunately, as K_L is increased the relaxation parameter α has to be decreased to satisfy the numerical stability criterion. With the most realistic run with $K_L = 10^7$ m^2 s^{-1}, it was found that α had to be less than 0.01. Furthermore, it required more than 100,000 underrelaxation steps for convergence errors to be less than 5%. This took 16 hours on one processor of a Cray-YMP, and hence to go to $K_L = 2 \times 10^8$ m^2 s^{-1} is computationally too expensive. As will be explained later, we feel that the results show signs of convergence with increasing K_L over our range of K_L. In future work it is of importance to develop a more efficient algorithm than underrelaxation so that realistic K_L values can be used.

The numerical algorithm was checked by using the case where $K_L = K_S$ and the ocean depth and geomagnetic field are uniform, in which case one should obtain uniform χ. The diffusion operator was checked also in this special case by comparing it with that obtained by performing the Laplacian operator using spherical harmonics.

7. The Ocean Model

The distribution of ocean currents was taken from a 2° × 2° version of the Geophysical Fluid Dynamics Laboratory (GFDL) ocean circulation model [*Bryan and Lewis*, 1979]. This particular version has over 30 levels in the vertical. The ocean circulation model is based on the primitive equations of motions with the Boussinesq approximation and hydro-

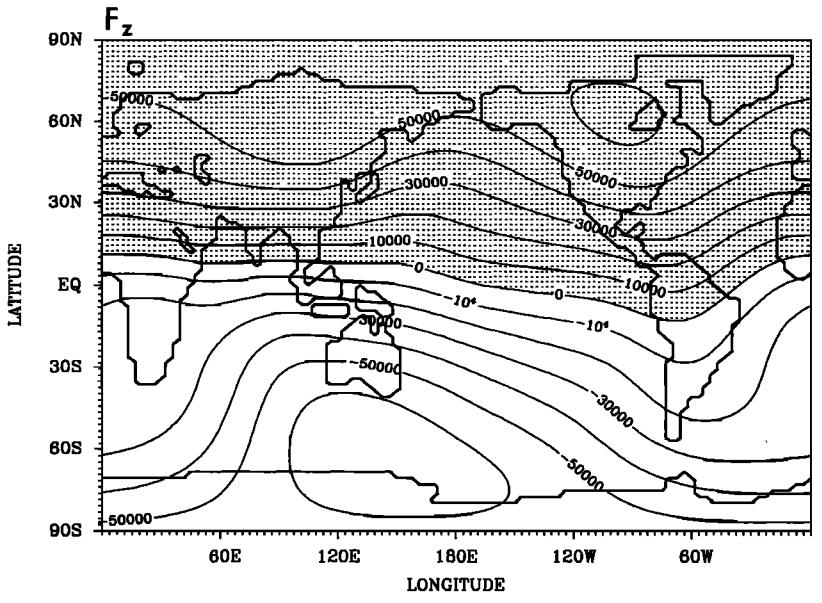

Fig. 1. The vertical component of the 1980 geomagnetic field, in nanoteslas.

static balance. Temperature, salinity, and wind stress are specified at the upper surface as a function from climatological data. The temperature and salinity were specified from a water mass atlas by *Levitus* [1982]. The wind stress data are taken from *Hellerman and Rosenstein* [1983]. The model is numerically integrated from an arbitrary initial state until it comes into approximate balance with the specified upper boundary conditions. In terms of resolution and configuration of boundary conditions, the experiment is similar to that of *Bryan and Lewis* [1979], but the vertical resolution is twice that of the earlier study.

Since the details of the electrical conductivity within the ocean are not explicitly considered in this preliminary study, the only output required of the model is the total transport and the depth distribution. The annually averaged pattern of the transport stream function is given in Figure 2. The most prominent feature is the Antarctic Circumpolar Current in the southern hemisphere, which is the ocean counterpart of the atmospheric jet streams. Continental barriers prevent a similar feature in the northern hemisphere. Westerlies and the trade winds provide anticyclonic torques in the subtropical zones of the oceans, giving rise to huge wind gyres, which have intensified poleward flowing boundary currents at the western side. The Kuroshio and the Gulf Stream are western boundary currents in the northern hemisphere, and the Brazil Current and the East Australian Current are similar features in the southern hemisphere.

Many features in Figure 2 can be explained by the simple theory of wind-driven currents [*Sverdrup*, 1947; *Godfrey*, 1989]. In some areas, however, the effect of topography is to horizontally separate the upper and lower branches of the thermohaline circulation. In this case the thermohaline cir-

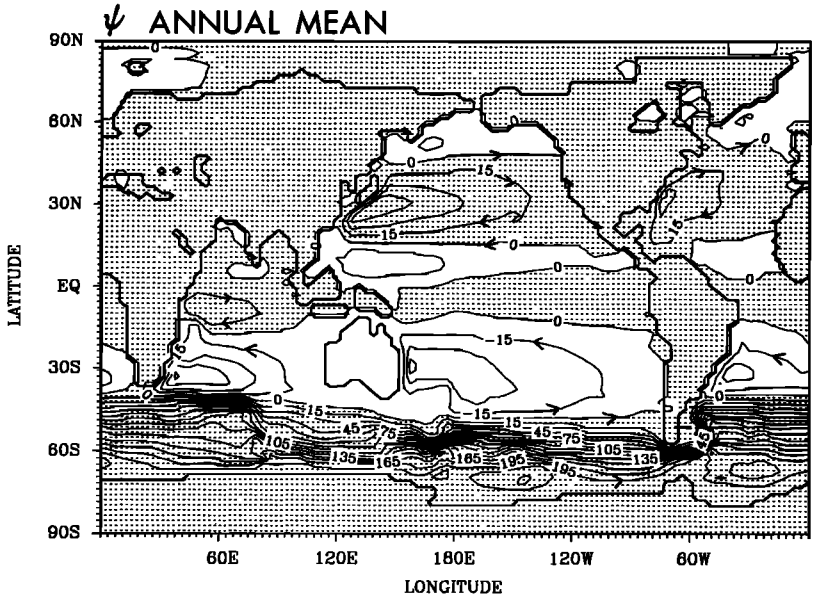

Fig. 2. The annual mean oceanic total transport stream function, in megatons per second.

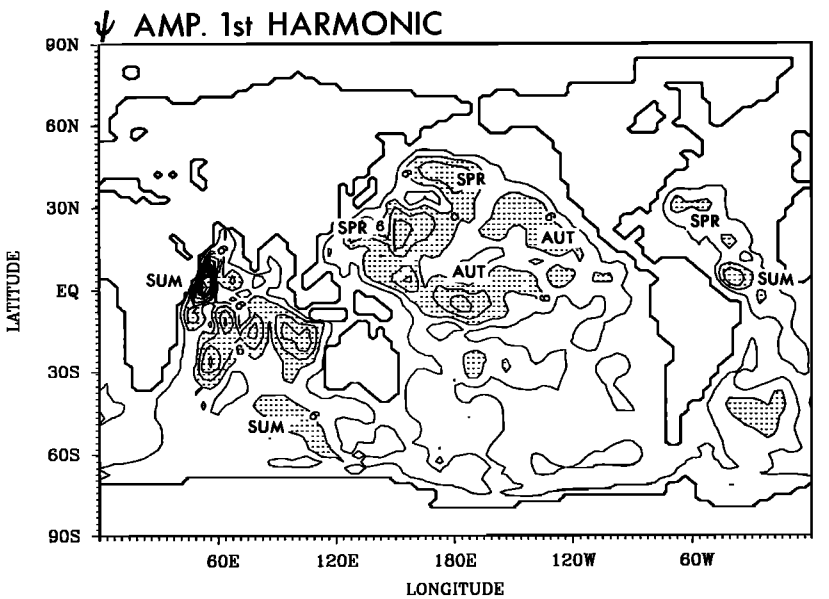

Fig. 3. The magnitude of the first annual harmonic of the total transport stream function, in megatons per second. Periods of maximum amplitude are denoted by WIN, SPR, SUM, and AUT signifying the northern winter, spring, summer, and autumn seasons, respectively.

culation is projected on to the barotropic component of the flow and influences the pattern of transport. This is particularly true in the North Atlantic.

Of particular interest for the present study is the amplitude of the first annual harmonic shown in Figure 3. The largest areas of changed circulation lie in regions directly affected by the Eurasian monsoons in the western Pacific and Indian oceans. In the Indian Ocean the reversal of the trade winds by the monsoon gives rise to very strong seasonal variations, which actually cause a reversal of surface currents along the equator and in the Somali Current region. Note that in this region the amplitude of the first harmonic of the stream function is greater than the amplitude of the mean transport stream function. In the northwestern Pacific the seasonal change is roughly 30% of the annual mean. At 35°N, 20°N, and 10°S in the western Pacific, the amplitude of the seasonal variation is greatest where the annual mean is a minimum, suggesting that north-south shifts of the wind pattern rather than a change in amplitude are responsible for the seasonal change.

Surprisingly there are rather small changes in circulation in the North Atlantic at high latitudes. A much greater change is indicated in the South Atlantic, where the Antarctic Circumpolar Current swings northward downstream of the Drake Passage. Part of this variation is related to north-south swings in the confluence region between the Brazil Current and the Malvinas (Falkland) Current.

Just north of the equator in the western Atlantic and western Indian oceans there are two areas of strong seasonal variation, connected in the Atlantic with a northward current running along the coast of Brazil and in the Indian Ocean with the Somali Current. Both seasonal currents are strong at the surface and are closely associated with coastal upwelling. Both of these currents are at a maximum in early summer. In subtropical latitudes of the northern hemisphere the western boundary currents are at a maximum late winter or early spring.

In the southern hemisphere the direction of flow is reversed so a maximum of the stream function in subtropical gyres also takes place in boreal spring. However, this corresponds to a minimum amplitude of the anticyclonic flow, and the maximum anticyclonic flow in the subtropical gyre region actually takes place in austral spring.

8. Results

Unless stated otherwise, all the following results refer to the case where $K_L = 10^7$ m^2 s^{-1}. Similar behavior appears to be converging to this in the runs with smaller K_L. Table 2 shows the dipole Gauss coefficients for χ as K_L is varied. Note how they appear to converge as K_L is increased.

Figures 4, 5, and 6 show the annual mean values for the χ, b_z, and electrical potential Φ fields. It can be seen that Φ shows strongest variations in regions of strong ocean cur-

TABLE 2. Convergence of χ Dipole Gauss Coefficients

	K_L/K_S					
(l, m)	1	10	20	30	40	50
(1, 0) g	36	82	72	63	57	51
(1, 1) g	201	194	176	168	164	160
(1, 1) h	398	382	339	315	299	286

Units are nanotesla Earth radii.

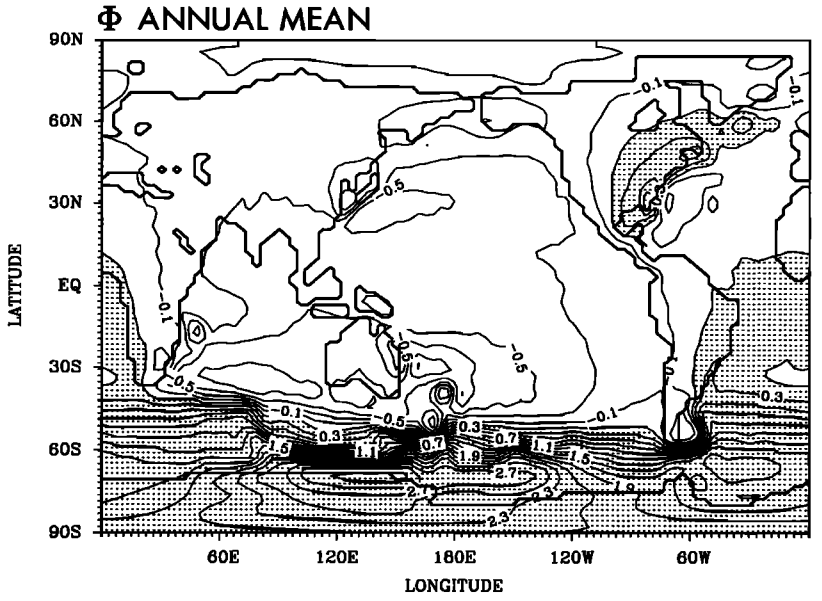

Fig. 4. The annual mean electric potential, in volts. Shading indicates values exceeding 0.1 V, and the contour interval is 0.2 V.

rents such as the Antarctic Circumpolar Current and the western boundary currents. The χ and b_z fields show largest values in regions where there are large depth variations and strong ocean currents. Note how in general the contours of the current density stream function avoid going through land areas and this is due to the low conductivity of land. Calculations were performed with a uniform ocean depth of D = 5500 m in all ocean areas, and the results were significantly different to these presented. The inclusion of variable bottom topography intensified the fields, especially Φ, and brought them into closer agreement with the values expected from naive scaling estimates discussed in section 5.

The electrical potential field shown in Figure 4 is the easiest field to interpret physically. Equations (20) and (21) require a relationship between the electric potential and ocean currents. As one faces downstream in the northern magnetic hemisphere, the highest potential should be on the left. In the southern magnetic hemisphere the highest potential should be to the right facing downstream. Note that the highest values are all at coasts in the northern hemisphere, since the strongest currents and the shallowest ocean depths are found there. The peaks in the potential near Madagascar and New Zealand may be spurious, since the ocean model required these areas to be shallow plateaus in the ocean rather than islands, and such a feature should excite a large electric field.

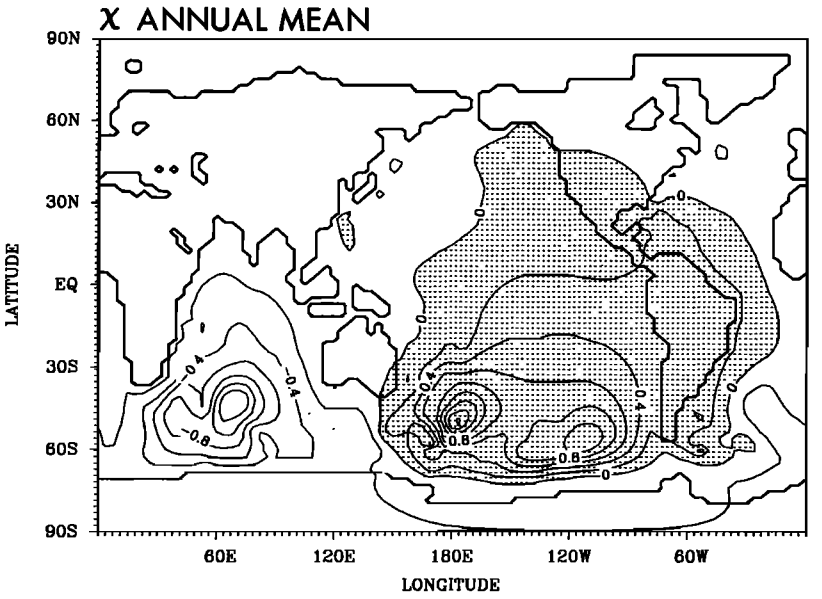

Fig. 5. The annual mean vertically integrated electric current density stream function, in nanotesla Earth radii. Shading is for values above zero, and the contour interval is 0.2 nT a. The arrows indicate the direction of electric current flow.

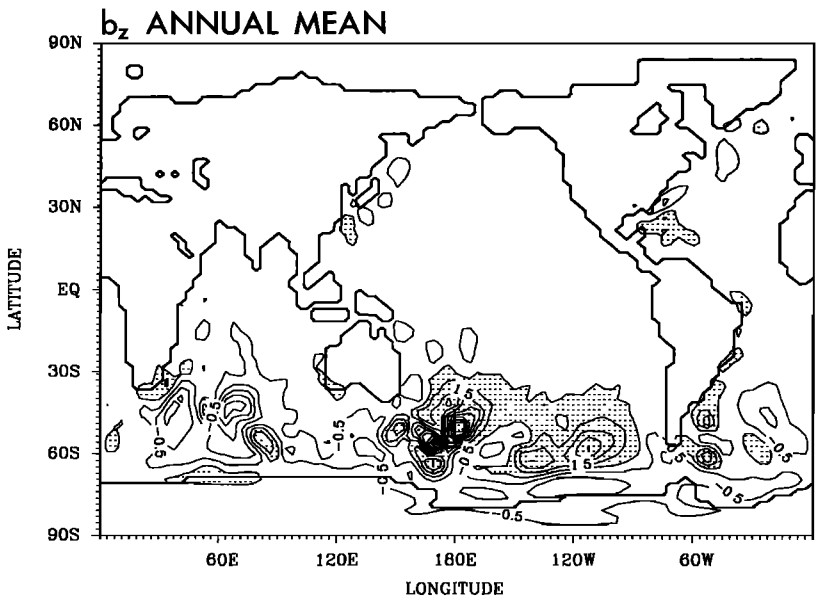

Fig. 6. The annual mean vertical component of the ocean-generated magnetic field at sea level, in nanoteslas. Shading indicates values above 0.5 nT, and the contour interval is 1 nT.

The stream function of the integrated current density, χ, shown in Figure 5, is rather weak along the western boundaries of the Atlantic and Pacific where the electric field has maximum gradients. As is shown in (23), the χ is forced only when lines of ψ and lines of $F_z K_{\text{eff}}/K_S$ do not coincide. Since K_{eff} is largely a function of depth, this implies that χ will not be excited unless lines of flow cut across bottom contours. Since the mean flow along the western boundaries of the North Atlantic and North Pacific is roughly aligned with bottom topography, the χ field is rather weak. In the Antarctic Circumpolar Current the flow is forced across submarine ridges in several places, and we see extrema in χ created near the Kerguelen Islands, the Macquarie Rise, the East Pacific Rise, and the Drake Passage.

The vertical component of the magnetic field generated by time-mean ocean currents is shown in Figure 6. It is closely related to the χ field, but is of even smaller scale. It is mainly confined to the southern ocean where the circulation is strongest, and the Antarctic Circumpolar Current tends to cut across isobaths. The contours are given in units of 0.5 nT and the maximum values are less than 5 nT. This value is less than that expected from naive scaling estimates, for example, 2 nT in the Gulf Stream rather than the expected 20 nT. One reason for this may be geometrical factors. For certain geometries the electric currents can be identically zero (e.g., the infinite uniform channel), and hence the scaling arguments provide only an upper bound. Another reason could be that our model only resolves scales greater than 2° and in a higher-resolution model, ocean currents would be narrower and more intense, leading to stronger magnetic fields. The magnitudes of the other components of the magnetic field may be stronger. The values of the order of 1 nT will be extremely hard to separate from the much larger variations in observed magnetic fields (e.g., 100 nT for magnetic storms, 15 nT yr^{-1} secular geomagnetic variation). Hence it appears that it may be very difficult to use magnetic observations to deduce ocean flows.

Figures 7–9 show the magnitude and phase of the annual harmonic of the Φ, χ, and b_z fields. The phase is denoted by the lettering WIN, SPR, SUM, and AUT signifying northern winter, spring, summer, and autumn seasons, respectively, as the period in which maximum amplitude occurs. Note that the regions of maximum magnitude are not basin-wide modes but tend to be localized. Four regions which predominate are the north Australian coast, the western boundary of the Pacific, the western North Atlantic, and the Indian Ocean, which is dominated by the monsoons. The regions of maximum amplitude are not simply correlated with those in the ocean stream function ψ. Ocean depth and closeness to magnetic poles play a role.

It can be seen that the magnetic field produced by the ocean is an extremely noisy and local field. This is as expected from the presence of $1/L$ in the naive scaling expression for b_z presented in section 5. The Gauss coefficients for the annual mean and for the magnitude of the annual harmonic are presented in columns 3–6 of Table 1; $\langle g \rangle$ and $\langle h \rangle$ are the annual mean values due to the ocean, and g' and h' are the magnitudes of the annual harmonic due to the ocean. It can be seen that the Gauss coefficients fail to diminish for the higher harmonics, unlike those for the geomagnetic field. This suggests that expansions of magnetic field station data in only a few spherical harmonics could lead to misleading results. From the scaling analysis one expects the strongest magnetic field to have the same horizontal scale as the strongest ocean currents. For the Gulf Stream this gives a length scale of roughly 200 km, which requires at least $l = 32$ for the highest harmonic.

The fact that the magnetic field is so local and is so small raises the question as to its effect in the calculation. If the electric currents were omitted in the calculation, would the calculated potential Φ still be correct? To address this question, consider the Φ calculated assuming the electric currents are zero:

$$\frac{\partial \Phi^0}{\partial \lambda} = \left(\frac{K_{\text{eff}}}{K_S}\right) \frac{F_z}{D} \frac{\partial \psi}{\partial \lambda} \tag{38}$$

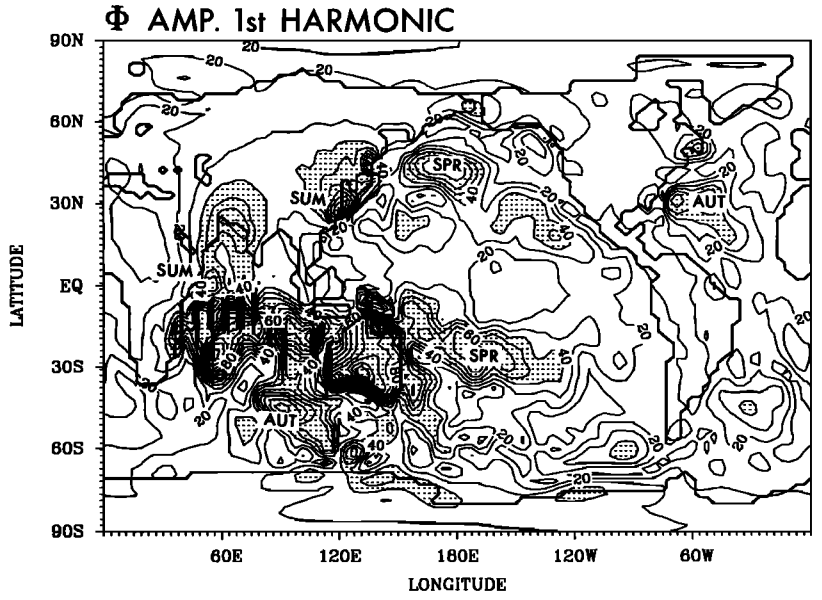

Fig. 7. The magnitude of the first annual harmonic of the electric potential, in volts. Shading indicates values above 40 mV and the contour interval is 10 mV.

$$\frac{\partial \Phi^0}{\partial \phi} = \left(\frac{K_{\text{eff}}}{K_S}\right) \frac{F_z}{D} \frac{\partial \psi}{\partial \phi} \tag{39}$$

This differs from the exact Φ by the difference in potential $\Phi^j = \Phi - \Phi^0$ which satisfies the equation

$$(a^2 \cos \phi) D \nabla^2 \Phi^j = \frac{\partial \chi}{\partial \phi} \frac{\partial K_{\text{eff}}}{\partial \lambda} - \frac{\partial \chi}{\partial \lambda} \frac{\partial K_{\text{eff}}}{\partial \phi} \tag{40}$$

In the case of the uniform K_{eff}, the potential associated with the electric currents Φ^j can be seen to be zero. However, in all other cases, Φ^j is not necessarily zero and should be calculated. Figures 10 and 11 show the annual mean and the magnitude of the annual harmonic of this potential. These figures can be compared with those of Φ in Figures 4 and 7. The annual mean of Φ^j is large in the vicinities of the New Zealand Plateau, the northern tropical Atlantic, and the western Pacific south of Japan. In these regions it is comparable to Φ in Figure 4, and hence in these regions electric currents are important in the calculation. The annual harmonic is sizable mainly in coastal regions where the depths are shallow, such as the Grand Banks on the east coast of America. At the Grand Banks the potential due to electric currents is 20 mV and is thus a large part of the 50 mV in the total potential variation at that point. To summarize, the hypothesis that the electric currents can be disregarded in calculating the electric potential is reasonable in many regions but does fail in certain regions. The regions in which it fails appear to be regions where flow is forced across

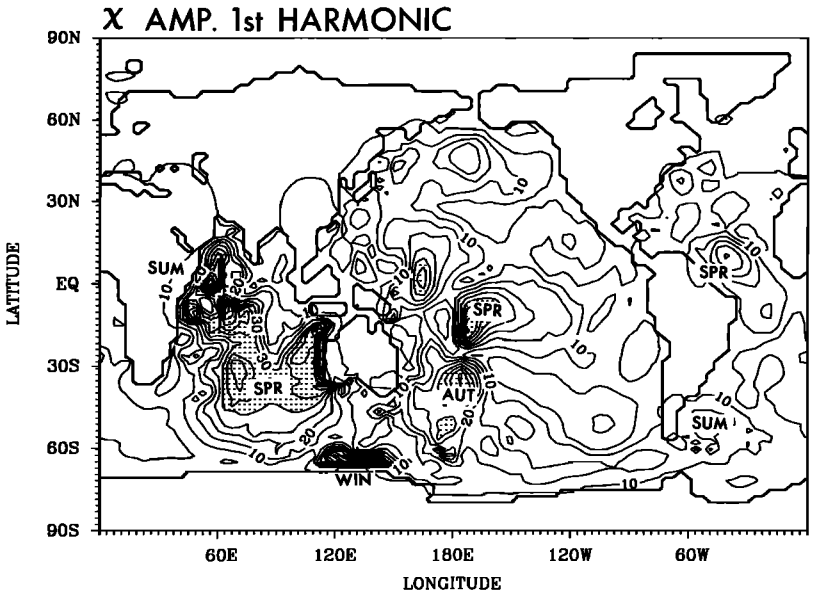

Fig. 8. The magnitude of the first annual harmonic of the vertically integrated electric current density stream function, in picotesla Earth radii. Shading is for values above 30 pT a, and the contour interval is 5 pT a.

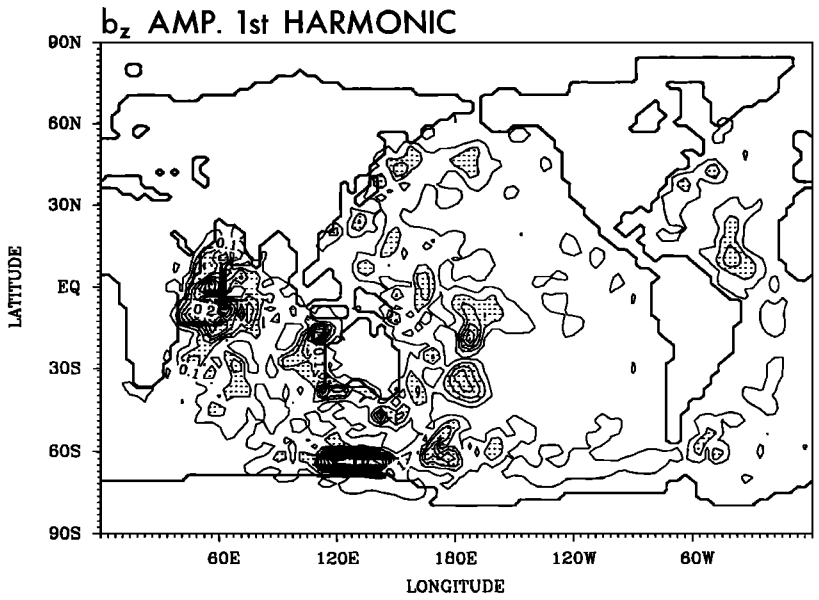

Fig. 9. The magnitude of the first annual harmonic of the vertical component of the sea level oceanic magnetic field, in nanoteslas. Shading indicates values above 0.1 nT, and the contour interval is 0.05 nT.

isobaths such as the New Zealand Plateau, the Kerguelen Plateau, and the Mid-Atlantic Ridge.

9. Discussion

We have derived consistent vertically integrated thin-shell equations capable of describing the electric and magnetic fields generated by the large-scale, low-frequency ocean flow using an idealized model of conductivity in the ocean and upper mantle. These have been solved numerically using data from a 2° × 2° ocean model in order to find the behavior of the annual mean and the first annual harmonic. The annual mean response is in accordance with scaling arguments which agree with previous values in the literature. The annual harmonic shows strong responses only in localized regions, and rather than being basin-wide, the response appears to be localized in regions of shallow depth and in regions with strong depth variations and strong barotropic currents. The magnetic field shows a lot of small-scale structure as expected from scaling arguments. In calculating the electric potential, the electric currents appear to play a small role in the calculation except in certain regions where transport lines cut across depth contours. In these regions, knowledge of both the electric and magnetic field would be necessary in order to deduce the ocean flow.

The fact that electric currents are generated when there is transport across isobaths has been mentioned previously in *Sanford*'s [1971] discussion of J^*. The work in this paper which allows us to numerically simulate the electromagnetic behavior of the ocean is complementary to the more analytical work of Sanford. It would be useful and interesting to

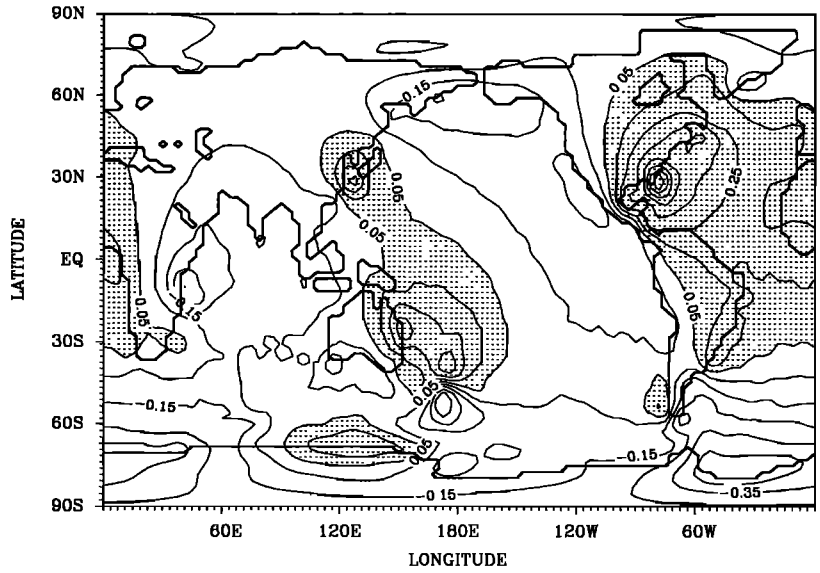

Fig. 10. The annual mean electric potential due to electric currents, in volts. Shading indicates values above 0.05 V, and the contour interval is 0.1 V.

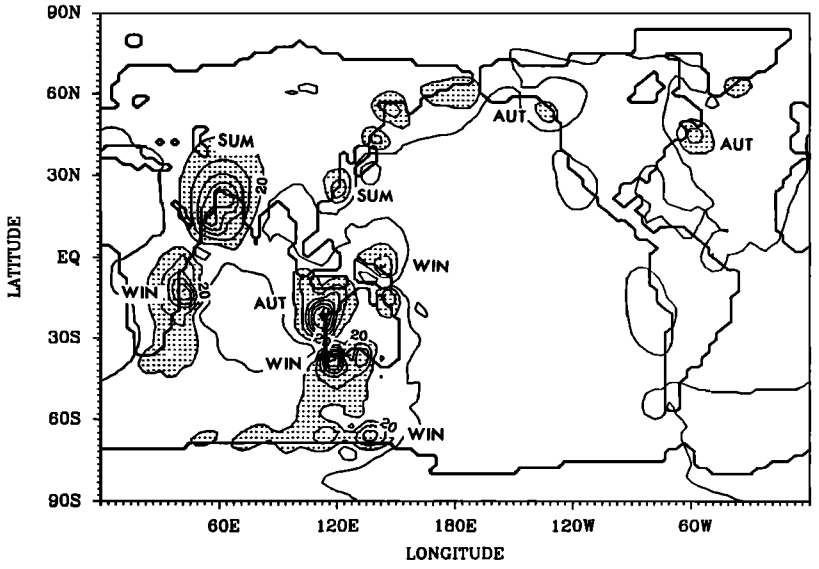

Fig. 11. The magnitude of the first annual harmonic of the electric potential due to electric currents, in volts. Shading indicates values above 20 mV, and the contour interval is 10 mV.

test these two methods on a more idealized case in order to obtain more insight into the electric currents J^*. Within the limitations of our model, and its simplified assumptions about conductivity, it appears that electric currents are large enough in some parts of the world ocean to make the electric field differ significantly from the naive case where electric currents are neglected entirely. This far from invalidates the useful electric field measurements of ocean transport but suggests that it would be useful to perform numerical modeling in regions where electric field measurements are being made. Sufficiently refined models could be useful in locating good sites for electromagnetic measurements.

The fact that the motionally induced magnetic field appears to have a lot of small-scale structure and is not easily related to the ocean flow suggests that magnetic field measurements may be a poor way to deduce large-scale ocean flow. Furthermore, the small signal strengths of the order of 1 nT are extremely prone to contamination from other geophysical sources such as magnetic storms and ionospheric jet fluctuations.

The electric field has strong signals of the order of 10 mV km^{-1} and in most regions is a direct result of the motion; i.e., electric currents are negligible. Hence the electric potential appears to be a good candidate for monitoring ocean flows. In designing a monitoring system it will be necessary to make preliminary direct measurements and solve the vertically averaged thin-shell equations for each site in order to ascertain the importance of electric currents. If the electric currents are found to be not negligible, then the inverse problem of deducing the flow from the electric potential could prove to be very difficult if not impossible. Certain regions such as the Kuroshio, the Gulf Stream at 50°N, the region north of Australia, and the region between Madagascar and Mazambique have a strong electric potential annual harmonic, and the flow is aligned with isobaths. Neglecting other factors of practical importance, these may prove to be regions where electric field measurements would be most useful.

Appendix A: Derivation of the Thin-Shell Approximation

For scaling purposes, let

$$\mathbf{F} = F_0\mathbf{F}' \qquad \mathbf{b} = F_0\beta\mathbf{b}' \qquad \mathbf{E} = \mathbf{U}F_0\mathbf{e}'$$

$$\mathbf{v} = U_0\mathbf{v}' \qquad K = U_0 a/R_m \qquad z = \delta a z'$$

$$t = (a/U_0)t' \qquad \nabla\Lambda = (1/a\delta)\nabla'\Lambda$$

where a is the radius of the Earth, δ is the ratio of the maximum depth of the ocean to a, β is the ratio of the magnitude $\mathbf{b}$ to the magnitude of $\mathbf{F}$, U_0 is a typical ocean velocity of 0.1 m s^{-1}, and F_0 is the magnitude of the geomagnetic field F. The primed quantities are nondimensional and of the order of unity. Both β and δ are small parameters of the order of $\varepsilon \sim 10^{-3}$, and hence we expected a power series expansion in them to converge quickly. The time scale a/U_0 is approximately 2 years. For much shorter time scales (less than hours), t' is significantly less than unity, and self-inductive effects become important, as can be seen in the following analysis. We are interested in the variations with a period of 1 year, and so t' is of the order of unity.

Equation (5) in section 2 may be expressed in terms of two equations

$$\mathbf{E} = K\nabla\Lambda\mathbf{b} - \mathbf{v}\Lambda(\mathbf{b} + \mathbf{F}) \tag{A1}$$

$$\partial\mathbf{b}/\partial t = -\nabla\Lambda\mathbf{E} \tag{A2}$$

In nondimensional form, (A1) and (A2) become

$$\beta\delta\frac{\partial\mathbf{b}'}{\partial t} = -\nabla' \times \mathbf{e}' \tag{A3}$$

$$e' = \frac{1}{R_m}\frac{\beta}{\delta}\nabla' \times \mathbf{b}' - \mathbf{v} \times (\beta\mathbf{b}' + \mathbf{F}') \tag{A4}$$

Naive inspection of (A3) and (A4) shows that the self-induction term is of the order of ε^2, the resistive term is of the order of ε^0, the dynamo term is of the order of ε^1, and the motional induction term is of the order of ε^0. Hence the ε^0 balance is expected to occur between only the resistive and the motional induction terms.

We can expand the operator $\nabla'\Lambda$ in terms of a power series in δ:

$$\nabla'\Lambda = \nabla^{(0)}\Lambda + \delta\nabla^{(1)}\Lambda - \delta^2 z'\nabla^{(1)}\Lambda + 0(\delta^3) \quad \text{(A5)}$$

where if $\mathbf{a} = (a_\lambda, a_\phi, a_z)$, then

$$\nabla^{(0)}\Lambda\mathbf{a} = \left(-\frac{\partial a_\phi}{\partial z'}, \frac{\partial a_\lambda}{\partial z'}, 0\right) \quad \text{(A6)}$$

$$\nabla^{(1)}\Lambda\mathbf{a} = \left[\frac{\partial a_z}{\partial \phi} - a_\phi, -\frac{1}{\cos\phi}\frac{\partial a_z}{\partial \lambda} + a_\lambda, \frac{1}{\cos\phi}\frac{\partial a_\phi}{\partial \lambda} - \frac{1}{\cos\phi}\frac{\partial}{\partial \phi}(a_\lambda \cos\phi)\right] \quad \text{(A7)}$$

Substituting these expressions into (A3) and (A4) and retaining only ε^0 terms (while noting that the z component of nondivergent fields such as $\mathbf{b}$ and $\mathbf{v}$ is of the order of δ less than the λ and ϕ components), gives

$$\partial e'_\phi/\partial z' = 0 \quad \text{(A8)}$$

$$\partial e'_\lambda/\partial z' = 0 \quad \text{(A9)}$$

$$\frac{1}{\cos\phi}\frac{\partial e'_\phi}{\partial \lambda} - \frac{1}{\cos\phi}\frac{\partial}{\partial \phi}(e'_\lambda \cos\phi) = 0 \quad \text{(A10)}$$

$$e'_\lambda = -\left(\frac{\beta}{\delta}\right)\frac{1}{R_m}\frac{\partial b'_\phi}{\partial z'} - v'F'_z \quad \text{(A11)}$$

$$e'_\phi = \left(\frac{\beta}{\delta}\right)\frac{1}{R_m}\frac{\partial b'_\lambda}{\partial z'} + u'F'_z \quad \text{(A12)}$$

These are the thin-shell equations, which should be a good representation of the magnetostatic equations when the shell is thin, the ocean magnetic field is small, and the time scale is much longer than the self-inductive time scale D^2/K.

Appendix B: Deducing the Observable Magnetic Field From the Magnetic Potential Drop

Let the magnetic scalar potential Ω be denoted by Ω^i for $r \le a - D$ and Ω^e for $r \ge a$. Expand the fields in terms of spherical harmonics:

$$\Omega^i(\lambda, \phi, r) = \sum_{l,m} Y_{lm}(\lambda, \phi)\omega^i_{lm} r^l \quad \text{(B1)}$$

$$\Omega^e(\lambda, \phi, r) = \sum_{l,m} Y_{lm}(\lambda, \phi)\omega^e_{lm} r^{-(l+1)} \quad \text{(B2)}$$

$$\chi(\lambda, \phi) = \sum_{l,m} Y_{lm}(\lambda, \phi)c_{lm} \quad \text{(B3)}$$

$$b_z = \sum_{l,m} Y_{lm}(\lambda, \phi)b_{lm} \quad \text{(B4)}$$

where m is the zonal wave number, and l is the total angular wave number. Using the boundary conditions $\Omega|^a_{a-D} = \chi$ and $\partial_r\Omega|^a_{a-D} = 0$ gives

$$\omega^e_{lm} a^{-(l+1)} - \omega^i_{lm} a^l = c_{lm} \quad \text{(B5)}$$

$$(l+1)\omega^e_{lm} a^{-(l+2)} + l\omega^i_{lm} a^{(l-1)} = 0 \quad \text{(B6)}$$

Physically, these boundary conditions are equivalent to a uniform vertical component of the magnetic field through the depth of the ocean but a jump condition in the potential.

These can be solved to find

$$\omega^e_{lm} = \frac{l}{(2l+1)} a^{(l+1)} c_{lm} \quad \text{(B7)}$$

$$\omega^i_{lm} = \frac{(l+1)}{(2l+1)} a^{-1} c_{lm} \quad \text{(B8)}$$

Using the fact that $b_z = \partial_r\Omega|_{r=a}$ gives

$$b_{lm} = -\frac{l(l+1)}{(2l+1)}\frac{c_{lm}}{a} \quad \text{(B9)}$$

Hence we have found the coefficient for the magnetic field b_{lm} given the coefficient c_{lm} for the magnetic potential drop χ. The spherical transforms are performed numerically using Gaussian quadrature.

Acknowledgments. The authors sincerely appreciate the help and encouragement they received from Keith Runcorn and Denis Winch, whose ideas on the effect of the ocean circulation initiated this study. Very helpful suggestions for improving the manuscript were also received from Charles Cox, James Larsen, and Thomas Sanford. James Girton played a significant role in carrying out our calculations.

References

Bryan, K., and L. J. Lewis, A water mass model of the world ocean, *J. Geophys. Res.*, *84*(C5), 2503–2517, 1979.

Chapman, S., and J. Bartels, *Geomagnetism*, vol. 2, Oxford at the Clarendon Press, London, 1940.

Chave, A. D., and D. S. Luther, Low frequency, motionally induced electromagnetic fields in the ocean, I, Theory, *J. Geophys. Res.*, *95*(C5), 7185–7200, 1990.

Cox, C. S., S. C. Constable, A. D. Chave, and S. C. Webb, Controlled source electromagnetic sounding of the oceanic lithosphere, *Nature*, *320*, 52–54, 1986.

Faraday, M., Experimental researches in electricity (Bakerian lecture), *Philos. Trans. R. Soc. London*, *122*, 163–177, 1832.

Godfrey, J. S., A Sverdrup model of the depth-integrated flow of the world ocean allowing for island circulations, *Geophys. Astrophys. Fluid Dyn.*, *45*, 89–112, 1989.

Hellerman, S., and M. Rosenstein, Normal monthly wind stress over the world ocean with error estimates, *J. Phys. Oceanogr.*, *13*(7), 1093–1104, 1983.

Larsen, J., Transport and heat flux of the Florida Current at 27°N derived from cross-stream voltages and profiling data: Theory and observations, *Philos. Trans. R. Soc. London, Ser. A*, *338*, 169–236, 1992.

Levitus, S., Climatological atlas of the world ocean, *NOAA Prof. Pap. 13*, 173 pp., U.S. Dep. of Commer., Washington, D. C., 1982.

Luther, D. S., J. H. Filloux, and A. D. Chave, Low-frequency, motionally induced electromagnetic fields in the ocean, II, Electric field and Eulerian current comparison, *J. Geophys. Res.*, *96*(C7), 12,797–12,814, 1991.

Mackie, R. L., B. R. Bennett, and T. R. Madden, Long period

magnetotelluric measurements near the central California coast: A land-locked view of the conductivity structure under the Pacific Ocean, *Geophys. J. Oxford*, *95*, 181–194, 1988.

Merrill, R. T., and M. W. McElhinney, *The Earth's Magnetic Field: Its History, Origin and Planetary Perspective*, Academic, San Diego, Calif., 1983.

Richtmyer, R. D., and K. W. Morton, *Difference Methods for Initial-Value Problems*, 405 pp., Interscience, 1967.

Sanford, T. B., Motionally-induced electric and magnetic fields in the sea, *J. Geophys. Res.*, *76*, 3476–3492, 1971.

Sverdrup, H. U., Wind-driven currents in a baroclinic ocean: With application to the equatorial currents of the eastern Pacific, *Proc. Natl. Acad. Sci. U.S.A.*, *33*, 318–326, 1947.

K. Bryan, Geophysical Fluid Dynamics Laboratory, NOAA, P.O. Box 308, Princeton University, Princeton, NJ 08542.

D. Stephenson, Department of Meteorology, University of Reading, Whiteknights, Reading, England RG6 2AU.

(Received February 28, 1992;
revised June 3, 1992;
accepted June 4, 1992.)